Band structure of diluted magnetic $Pb_{1-x}Mn_xTe$: Magneto-optical investigations and four-wave-mixing spectroscopy

H. Pascher and P. Röthlein
Physikalisches Institut, Universität Bayreuth, Postfach 10 12 51, D-8580 Bayreuth, Federal Republic of Germany

G. Bauer
Institut für Physik, Montanuniversität Leoben, A-8700 Leoben, Austria

M. von Ortenberg
Institut für Halbleiterphysik und Optik, Technische Universität Braunschweig, D-3300 Braunschweig, Federal Republic of Germany

(Received 15 March 1989; revised manuscript received 24 July 1989)

Magneto-optical intraband and interband experiments on epitaxial $Pb_{1-x}Mn_xTe$ samples with Mn contents $x \leq 2\%$ are reported. A direct observation of spin-flip transitions of electrons and holes is performed down to magnetic fields of less than 0.05 T by using coherent anti-Stokes Raman scattering experiments. g factors are determined as a function of magnetic field as well as a function of temperature. All experimental data are well accounted for by treating the exchange interaction between the mobile carriers and the localized $3d$ electrons of the Mn^{2+} ions in a mean-field approximation. In this many-valley semiconductor with conduction- and valence-band extrema at the L point of the Brillouin zone, four exchange integrals are relevant. These integrals have opposite influence for the conduction and valence bands, and the exchange-induced effects are much larger for holes than for electrons. The data and their interpretation yield conclusive evidence against the "zero-field splitting," i.e., a finite energy difference of spin-split states in zero magnetic field ("free magnetic polaron") in $Pb_{1-x}Mn_xTe$ with $x < 0.02$. The upper limit for the binding energy of a free magnetic polaron, if it exists at all, is less than 0.05 meV in $Pb_{1-x}Mn_xTe$, a value determined by the remaining experimental uncertainty. Although the experimental magneto-optical transition energies are perfectly fitted by the molecular-field approximation, their temperature dependence reveals the necessity for temperature-dependent exchange parameters, which is beyond a mean-field approach.

I. INTRODUCTION

Diluted magnetic semiconductors (DMS), or "semimagnetic" semiconductors, are semiconducting alloys with substitutional magnetic ions. They exhibit a variety of interesting magnetic, magneto-optical, and transport properties.[1]

Apart from $A^{II}_{1-x}Mn_xB^{VI}$ compounds, diluted magnetic cubic IV-VI compounds which crystallize in the rock-salt structure have attracted considerable interest.[2] The incorporation of Mn^{2+} or Eu^{2+} into the PbTe (Ref. 3) or PbSe (Ref. 4) lattice causes a more or less rapid increase of the energy gap with the paramagnetic-ion content.

It was found that the antiferromagnetic interaction between the Mn^{2+} ions in the IV-VI materials[5,6] is smaller than that in the corresponding narrow-band-gap II-VI compounds. The Eu-Eu exchange effects in $Pb_{1-x}Eu_xTe$ are even weaker than the Mn-Mn interaction in IV-VI host materials, as expected.[7] However, in a quaternary (or pseudobinary) IV-VI compound, in $Pb_{1-x-y}Sn_yMn_xTe$ with high tin contents ($y \approx 0.7$) a carrier concentration ($p > 10^{20}$ cm^{-3}) induced paramagnetic-ferromagnetic transition was found.[8,9] Thus, in the magnetic phase diagram the carrier concentration is an additional parameter apart from the Mn content and the temperature, an effect so far only found in the IV-VI-compound-based DMS. Recently, also in $Pb_{1-x}Eu_xSe$ with Eu contents x above 2%, evidence for magnetic ordering effects were observed.[10]

The first investigation on the exchange interaction between free carriers and localized Mn spins in $Pb_{1-x}Mn_xTe$ was performed by Kossut *et al.*[11] Subsequently investigations on transport and cyclotron resonance,[12] interband magneto-optical transitions in $Pb_{1-x}Mn_xTe$ (Ref. 13), and laser emission in $Pb_{1-x}Mn_xS$ (Ref. 14) were carried out. Karczewski and von Ortenberg[15] even deduced a zero magnetic-field splitting of the energy gap in $Pb_{1-x}Mn_xS$ from the laser emission experiments. From their magneto-optical experiments Pascher *et al.*[13] concluded that there is an additional contribution to the spin splitting of Landau states which is nearly independent of applied field between about 1 and 7 T. The experimental interband data on $Pb_{1-x}Mn_xTe$ extrapolated from the high-field region to zero magnetic field resulted in a nonvanishing spin splitting of the valence-band states. Consequently it was concluded that the mean-field approach, in which the carriers experience an averaged

effective field of the Mn spins, is insufficient for the proper description of the IV-VI compound DMS materials.[16]

It is the purpose of this paper to report systematic studies on magneto-optical properties using *n*- and *p*-type $Pb_{1-x}Mn_xTe$ samples with $0.006 \leq x \leq 0.019$. For this range of compositions the magnetic properties are by now well understood.[17]

In Sec. II we sketch the mean-field theory of the exchange interaction in cubic IV-VI compounds; in Sec. III experimental details are presented. Results on magneto-optical interband and intraband experiments are presented in Sec. IV together with their analysis. In this section also spin-resonant four-photon mixing experiments are described which give extremely precise information on the magnetic field and temperature dependence of spin-split states both in the conduction as well as the valence band. In Sec. V we discuss the determination of the band structure and of the four exchange parameters. A detailed discussion on the temperature and magnetic-field dependence of the *g* factors for electrons and holes is given. In Sec. VI, the Conclusion, we summarize our experimental and theoretical findings.

II. CALCULATION OF LANDAU STATES: MEAN-FIELD THEORY FOR IV-VI COMPOUNDS

The $\mathbf{k}\cdot\mathbf{p}$ band model for the lead compounds has been derived by several authors. In the following we use the notation of Adler *et al.*[10] which treat exactly the interaction of the upper most valence-band and the lowest conduction-band level, whereas the interaction with two more distinct conduction and valence levels is treated in k^3 approximation. The 4×4 matrix Hamiltonian for the calculation of the Landau states resulting from this procedure is given in Ref. 18.

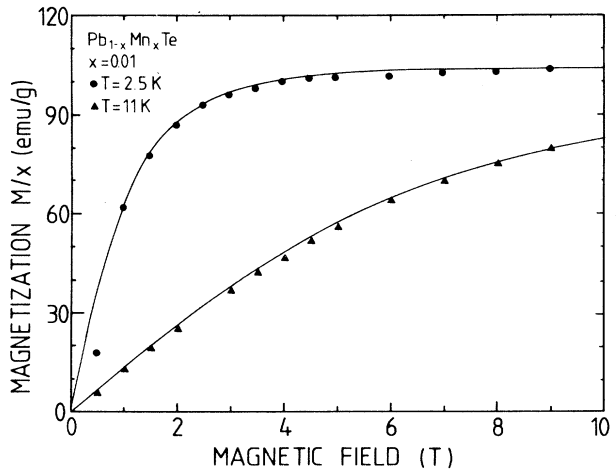

FIG. 1. Magnetization vs temperature for $Pb_{1-x}Mn_xTe$, $x=0.01$. Experimental data for $T=2.5$ K (●) and $T=11$ K (▲). Solid lines: Results of calculation using modified Brillouin function [$T_0(2.5\ \text{K})=0.7$ K, $S_0=2.25$; $T_0(11\ \text{K})=0.15$, $S_0=2.25$].

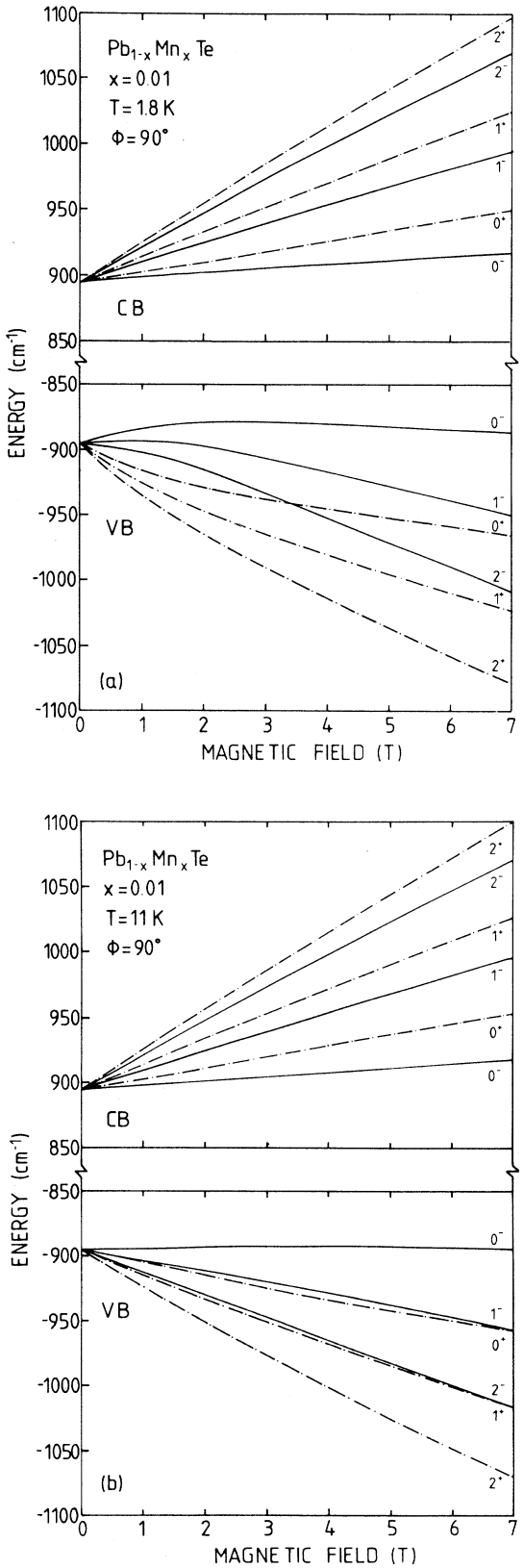

FIG. 2. (a) Dependence of Landau states in the conduction band of $Pb_{1-x}Mn_xTe$ (for $\Phi=90°$) and in the valence band on the magnetic field for $T=1.8$ K. (b) As in (a) but for $T=11$ K.

For $Pb_{1-x}Mn_xTe$ with rather small Mn contents x we assume that the sequence of energy levels is not altered with respect to PbTe. In the spirit of the mean-field approximation[19] (MFA) an exchange matrix is added to the 4×4 matrix Hamiltonian.[12,13,20,21] This 4×4 exchange matrix contains off-diagonal terms which cause a strong mixing of Landau states with different spin and Landau quantum numbers. In order to calculate the energies of the 0^+ and 0^- Landau states of the conduction and valence bands a 12×12 Hamiltonian $\tilde{\mathcal{H}}=\tilde{\mathcal{X}}+\tilde{\mathcal{Y}}$ is used where $\tilde{\mathcal{X}}$ has three 4×4 blocks according to Eq. (8) of Ref. 18 along the main diagonal for the Landau quantum numbers $n=-1$, 0, and $+1$.

The exchange matrix $\tilde{\mathcal{Y}}$ is given by Eq. (1) of Ref. 21. It contains the modified Brillouin function with S_0 and T_0 as fit parameters usually determined from magnetization data.[5] The matrix elements a,c and b,d are functions of four exchange parameters as defined in Refs. 12, 13, and 20 for the valence (A,a_1) and conduction band (B,b_1), respectively. These exchange parameters depend on the four exchange integrals, four spin-orbit mixing parameters $\sin^2\Theta^{\pm}$, $\cos^2\Theta^{\pm}$, and the angle γ for the rotation of the reference frame [see Ref. 18, Eq. (6)]. For this band symmetry, the four exchange integrals are given by[13]

$$\alpha=(R|J|R)/\Omega,\quad \delta=(S_{\pm}|J|S_{\pm})/\Omega\ ,$$
$$\beta_{\parallel}=(X_{\pm}|J|X_{\pm})/\Omega,\quad \beta_{\perp}=(Z|J|Z)/\Omega\ . \tag{1}$$

The symmetry properties of $X_{\pm},Z,R,S_{\pm}$ are defined in Ref. 18. J is the exchange-coupling constant. For the calculation of higher Landau states the schemes for $\tilde{\mathcal{X}}$ and $\tilde{\mathcal{Y}}$ have to be extended accordingly.

In order to determine S_0 and T_0, magnetization data as a function of magnetic field and temperature are necessary. In Fig. 1 theoretical magnetization curves calculated with the parameters given by Anderson and Gorska[5] are compared with experimental data for one of our samples. Using these data and the exchange parameters determined from fits to magneto-optical experiments in Figs. 2(a) and 2(b), Landau levels for the conduction and valence band are shown calculated for two temperatures and $\Phi=90°$. At $T=1.8$ K the exchange-induced corrections alter drastically the magnetic-field dependence of the Landau states causing even a positive slope of the 0^- valence-band level at small magnetic fields. For higher temperatures the influence of the exchange interaction decreases and the magnetic-field dependence of the Landau states resembles nearly the diamagnetic host material. It should be noted that the approach outlined above is only suitable for the momentum $k_B=0$.

III. EXPERIMENT

The $Pb_{1-x}Mn_xTe$ samples investigated were prepared by hot wall epitaxy (Elsinger *et al.*[22]), on cleaved BaF_2 substrates. The samples have contents x ranging from 0.7% to 1.9% carrier concentrations (n or p type) from 1.2×10^{17} to 3.8×10^{17} cm^{-3} and electron mobilities up to 3×10^5 cm^2/V s (at $T=4.2$ K for Mn contents about 1%). The hole mobilities are usually considerably lower than those of the electrons. The homogeneity of the Mn content as a function of sample thickness was checked by SIMS measurements, and it was found that in the epitaxial layers its variation with the $Pb_{1-x}Mn_xTe$ film thickness was less than 5% of the nominal Mn content.[23]

Magneto-optical interband transmission experiments were performed with the samples either immersed in superfluid helium or situated in an exchange-gas chamber, for magnetic-field orientations $\mathbf{B}\|\mathbf{k}\|[111]$ (Faraday geometry, using σ^+ and σ^- circularly polarized radiation) or in Voigt geometry with $\mathbf{B}\|[1\bar{1}0]\|\mathbf{E}$ or $\perp\mathbf{E}$ (linear polarization). The samples were oriented with respect to these orientations within an accuracy of 2°. For the measurement of the transmission versus magnetic field, either various CO-laser lines were used or those of a CO_2 laser frequency doubled with an appropriately cut Te crystal.[13]

The magneto-optical intraband experiments were performed either with a CO_2-laser-pumped far-infrared (FIR) laser employing light-pipe techniques and a Bitter magnet coil or Fourier transform spectroscopy with the sample situated in a split-coil magnet. Transmission experiments in Faraday ($\mathbf{B}\|\mathbf{k}\|[111]$, linear polarization) and Voigt geometry ($\mathbf{E}\|\mathbf{B}\|[1\bar{1}0]$, $\mathbf{k}\perp\mathbf{B}$, linear polarization) were performed.

In order to measure directly the temperature and magnetic-field dependence of the electron and hole g factors a setup for coherent anti-Stokes Raman scattering (CARS) experiments operating in the infrared was used. Two Q-switched CO_2 laser beams with frequencies ω_L and ω_S generate in the $Pb_{1-x}Mn_xTe$ sample radiation with frequencies at $\omega_L\pm i(\omega_L-\omega_s)$, i being an integer. The intensity at the anti-Stokes frequency $\omega_{AS}=2\omega_L-\omega_s$ is monitored as a function of magnetic field for several fixed combinations ω_L,ω_s. The intensity I_{AS} at ω_{AS} is proportional to the square of the nonlinear susceptibility χ, which causes a resonant enhancement of I_{AS}, whenever $\omega_L-\omega_s$ corresponds to a Raman allowed transition.[24] In a magnetic field with orientation $\mathbf{B}\perp\mathbf{k}$, i.e., in Voigt geometry, the most important resonance in the nonlinear susceptibility is a spin-flip resonance,[25]

$$\hbar(\omega_L-\omega_s)=g^*\mu_B B_{\rm res}\ , \tag{2}$$

where g^* is the effective g factor for the particular orientation of $\mathbf{B}$. The setup for the experiments is described in detail in Ref. 24. Because of the high peak powers (2.5 kW, 100 ns pulse duration) of the CO_2 lasers, minority carriers are photoexcited across the energy gap in n-type as well as in p-type samples, and their respective g factors can be determined together with those of the majority carriers.[20] As outlined in Ref. 24, in these experiments complicated line shapes occur due to the interference of the resonant and nonresonant parts of the susceptibility:

$$|\chi|^2=|\chi^{\rm NR}|^2+|\chi'|^2+|\chi''|^2+2\chi^{\rm NR}\chi'\ , \tag{3}$$

where $\chi^{\rm NR}$ denotes the nonresonant part (which is predominantly real in the frequency range of interest) and χ' and χ'' are the real and imaginary part of the resonant contribution. Therefore either intensity extrema or points of inflection correspond to the resonant magnetic

fields. Whether extrema or point of inflections have to be evaluated depends on the relative strengths of resonant in comparison to nonresonant contributions. In general, the resonant part is weak if the occupation difference of the two spin levels is small, which is the case either for small magnetic fields or for a small total number of carriers in the initial state. Then B_{res} corresponds to points of inflection. For dominant resonant contributions B_{res} has to be taken at the intensity maxima. Further details of the line-shape analysis of the CARS resonances are given in Ref. 24.

The CARS method offers the particular advantage that spin-split energies can be determined for magnetic field as low as 0.05 T which is extremely important for the investigation of the semimagnetic properties of $Pb_{1-x}Mn_xTe$.

IV. EXPERIMENTAL RESULTS AND ANALYSIS

A. Interband magneto-optical transitions

In Fig. 3 a typical magneto-optical interband transmission as a function of magnetic field is shown for the two circular polarizations σ^+ and σ^- in Faraday geometry for a p-type sample with $x=0.006$ at $\tilde{\nu}=1959.4\ cm^{-1}$. It is evident that the resonant magnetic fields which were taken to be at positions of the transmission minima are different for the two polarizations in contrast to the PbTe case. From a large number of such recordings taken of various infrared laser frequencies fan charts were obtained as shown in Fig. 4(a) for the Faraday configuration and in Fig. 4(b) for the Voigt configuration. The solid lines correspond to calculated transitions with the selection rules $\Delta n=0$, $\Delta s=\pm 1$ (Faraday geometry), $\Delta n=0$, and $\Delta s=0$ ($\mathbf{E}\|\mathbf{B}$). We would like to point out that the mean-field theory of Sec. II is capable of explaining nearly all of the experimental data, even delicate features like the crossing of several transitions as a function of B in Voigt geometry [see Fig. 4(b)]. In Ref. 13 we have argued that magneto-optical interband transitions provide some evidence for a "zero-field spin splitting," i.e., a splitting of 0^- $(,1^-,2^-,\ldots)$ and 0^+ $(,1^+,2^+,\ldots)$ states for $B\rightarrow 0$. We were led to this conclusion by a simple extrapolation of the experimentally observed interband transition energies from higher fields to $B\rightarrow 0$ both in Faraday and Voigt geometry. However, no experimental data below $B=1$ T were available. For temperatures as low as 1.8 K the change of magnetization with field (Fig. 1) is particularly strong and hence the influence of the exchange interaction of the Landau states as shown in Fig. 2. The bowing in the field dependence of the Landau states with small quantum numbers reflects itself in the curvature of the transition energies in both configurations.

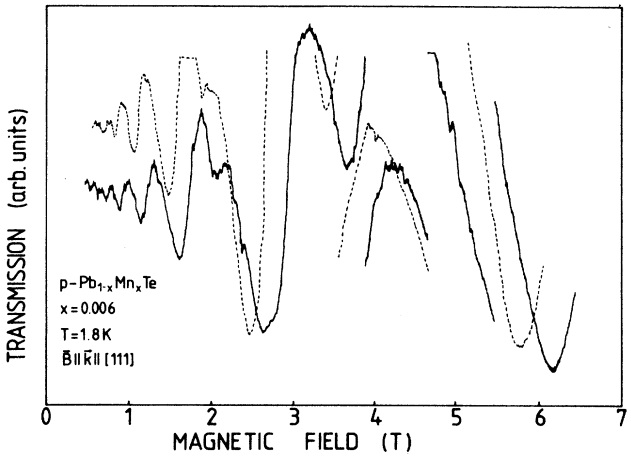

FIG. 3. Interband transmission vs magnetic field for $Pb_{1-x}Mn_xTe$ with $x=0.006$ at $T=1.8$ K in Faraday geometry; solid lines, σ^+ circularly polarized radiation; dashed lines, σ^- polarization.

In Faraday configuration, from the mere inspection of the high-field data alone one is led to the assumption of a magnetic-field-independent additional contribution to the spin splitting of the Landau states. The reason for this fact is evident from the data of Fig. 1, where the magnetization is already near saturation for $B\geq 2$ T even at $T=2.5$ K.

In Voigt geometry [Fig. 4(b)] one relatively strong series of interband transitions is observed which does not obey the selection rules $\Delta n=0$, $\Delta s=0$. It turns out that a transition 0^+ (VB)$\rightarrow 0^-$(CB), i.e., $\Delta s=-1$ is observed, within the $\Phi=35.26°$ valleys. Φ denotes the angle between the main valley axis of the surfaces of constant energy and the orientation of the magnetic field $\mathbf{B}$. The allowed transitions 0^+(VB)$\rightarrow 0^+$(CB) for $\Phi=35.26°$ also appears, whereas 0^-(VB)$\rightarrow 0^-$(CB) is blocked due to the position of the Fermi energy.

Experiments were performed on several samples with x values up to $x=1.9\%$. The band parameters from the fits are given in Table I, the far band parameters[18] were kept independent of the Mn content ($x\leq 0.012$) and are given as follows:

TABLE I. Band parameters.

Sample	PbTe	$Pb_{1-x}Mn_xTe$	$Pb_{1-x}Mn_xTe$	$Pb_{1-x}Mn_xTe$
x	0	0.006	0.01	0.012
E_g (meV)	189.7	209.8	221.9	225.7
$2P_\perp^2/m_0$ (eV)	6.02	5.77	5.51	
$P_\perp/P_\parallel$	3.42	3.52	3.74	

TABLE II. Exchange parameters.

Mn content	T (K)	A (meV)	a_1 (meV)	B (meV)	b_1 (meV)	T_0 (K)
$x=0.010$	1.8	-182 ± 15	-288 ± 15	-33 ± 10	27 ± 5	0.7
$x=0.008$	1.8	-192 ± 15	-315 ± 15	-66 ± 10	55 ± 5	0.4
$x=0.006$	1.8	-225 ± 15	-314 ± 15		50 ± 5	0.8
$x=0.006$	3.5	-142 ± 15	-279 ± 15	-41 ± 10	50 ± 5	1.0
$x=0.006$	4.4	-124 ± 15	-279 ± 15	-51 ± 10	51 ± 5	0.7
$x=0.006$	12.0	-51 ± 15	-288 ± 155		59 ± 5	0.5

$m_t^-/m_0=0.060$, $m_1^-/m_0=0.505$,

$m_t^+/m_0=0.102$, $m_1^+/m_0=0.920$,

$g_t^-=-1.39$, $g_1^-=1.72$,

$g_t^+=4.39$, $g_1^+=-2.61$

in Adler *et al.* notation.[18]

The exchange parameters are given in Table II. The exchange integral α (Ref. 20) turns out to be $\alpha=-305$ meV, independent of T (1.8–20 K) and of x ($x\leq0.010$). $\beta_{\|}^*$ is also independent of T and equals $+225$ meV (for $x=0.006$), whereas $\beta_{\perp}^*$ varies from 120 to 140 meV with

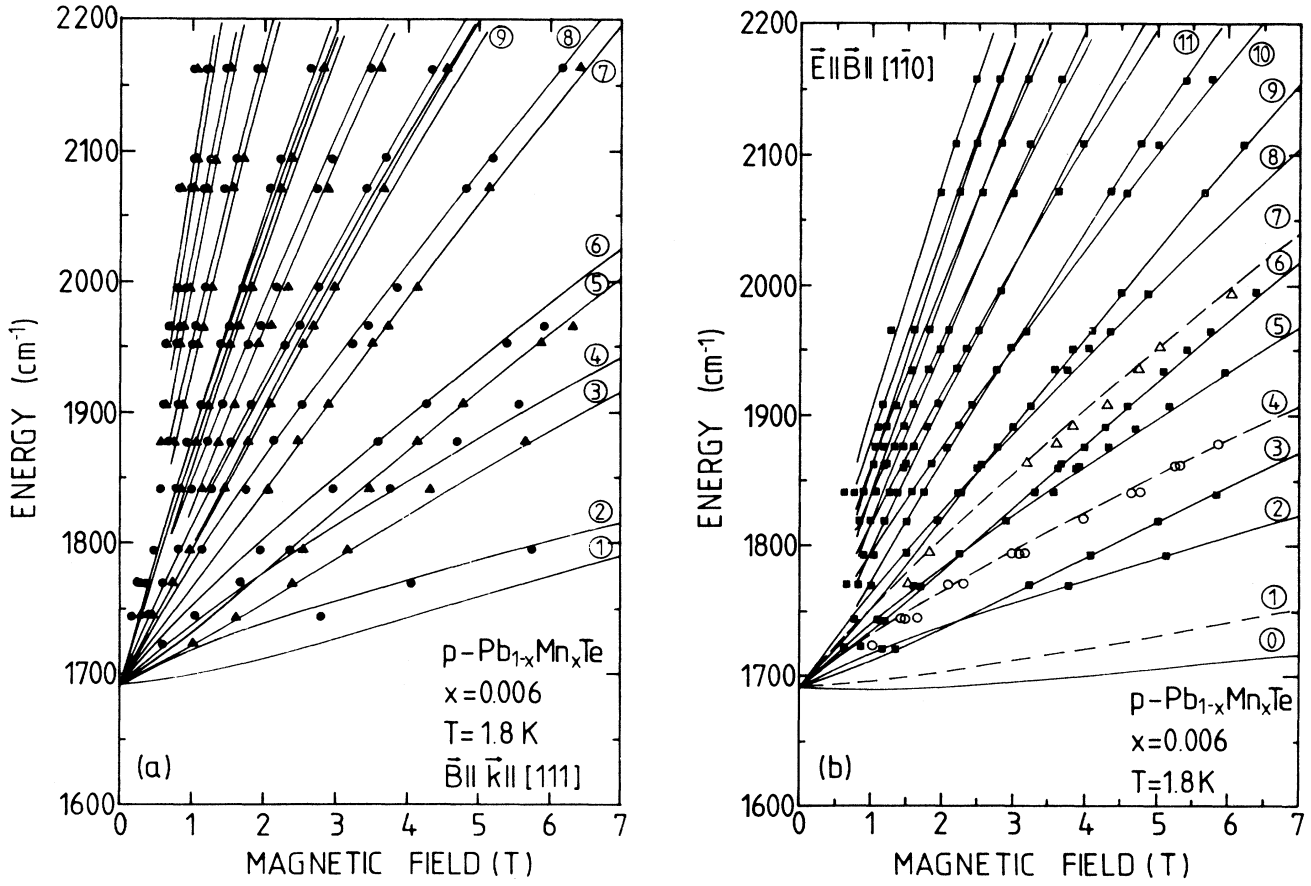

FIG. 4. (a) Fan chart for interband magneto-optical transitions in Faraday geometry. ●, ▲ experimental data (σ^-,σ^+). Solid lines, calculated data. Identification: 1, $0^-\rightarrow0^+(\Phi=70.53°)$; 2, $0^+\rightarrow0^-(\Phi=70.53°)$; 3, $0^-\rightarrow0^+(\Phi=0°)$; 4, $0^+\rightarrow0^-(\Phi=0°)$; 5, $1^-\rightarrow1^+(\Phi=70.53°)$; 6, $1^+\rightarrow1^-(\Phi=70.53°)$; 7, $2^-\rightarrow2^+(\Phi=70.53°)$; 8, $2^+\rightarrow2^-(\Phi=70.53°)$; 9, $1^-\rightarrow1^+(\Phi=0°)$; etc. (b) As in (a) but for Voigt geometry $\mathbf{B}\|[1\bar{1}0]$. Experimental data ■,Δ in $\mathbf{E}\|\mathbf{B}$ polarization. Solid lines, calculated data for $\Phi=90°$; dashed lines, $\Phi=35.26°$. 0, $0^-\rightarrow0^+(\Phi=90°)$; 1, $0^-\rightarrow0^-(\Phi=35.26°)$; 2, $0^+\rightarrow0^-(\Phi=90°)$; 3, $1^-\rightarrow1^-(\Phi=90°)$; 4, $0^+\rightarrow0^-(\Phi=35.26°)$; 5, $1^+\rightarrow1^+(\Phi=90°)$; 6, $2^-\rightarrow2^-(\Phi=90°)$; 7, $0^+\rightarrow0^+(\Phi=35.26°)$; 8, $2^+\rightarrow2^+(\Phi=90°)$; 9, $3^-\rightarrow3^-(\Phi=90°)$; 10, $3^+\rightarrow3^+(\Phi=90°)$; 11, $4^-\rightarrow4^-(\Phi=90°)$.

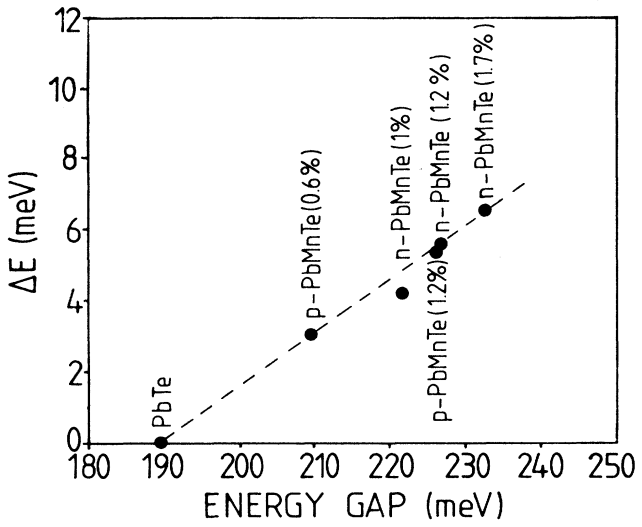

FIG. 5. Energy splitting between interband transitions in Faraday geometry (between σ^+ and σ^- transitions) at $B=3$ T for samples with different Mn content as a function of their energy gap.

T increasing up to 12.0 K. The value of δ (which is the most uncertain one) changes from -1700 meV at $T=1.8$ K to -5900 meV at $T=12$ K ($x=0.006$).

In Faraday geometry at higher fields in excess of about 2 T the transitions $n^+(\mathrm{VB})\rightarrow n^-(\mathrm{CB})$ as well as $n^-(\mathrm{VB})\rightarrow n^+(\mathrm{CB})$ have nearly identical slope. In PbTe these transitions almost coincide with each other. In Fig. 5 the energy difference between these two kinds of transitions, ΔE, is plotted versus the energy gap of the samples for the Mn contents up to 1.7%. With increasing Mn content ΔE increases for five different samples nearly linearly with the energy gaps.

B. Far-infrared spectroscopy

Magneto-optical intraband transitions in Faraday geometry were investigated in a number of n- and p-type samples to get independent information on the effective masses and their anisotropy. Earlier investigations on n- and p-type $Pb_{1-x}Mn_xTe$ were presented in Refs. 23, 12, 26, and 27. For $\mathbf{B}\|[111]$ two resonant frequencies associated with cyclotron transitions in the [111] ($\omega_{c1}, \Phi=0°$) and in the three obliquely oriented $\langle 111\rangle$ ($\Phi=70.53°$) valleys are expected. In samples with high mobility and consequently long relaxation times with FIR laser spectroscopy both $n^-\rightarrow(n+1)^-$, $n^+\rightarrow(n+1)^+$ transitions can be observed as shown in Fig. 6(a) for a n-type sample with $x=0.01$. The identification of the resonance frequencies is generally based on oscillator fits using a model dielectric function[28] since for laser energies $\hbar\omega_L$ below about 14 meV, $\hbar\omega_{TO}<\hbar\omega_L<\hbar\omega_{LO}$, where ω_{TO} and ω_{LO} denote the TO and LO optic-mode phonon frequencies. Thus, in this range the magnetotransmission experiments are performed in the reststrahlen region where the resonances are accompanied by dielectric anomalies. In addition for transition energies close to $\hbar\omega_{LO}+E_F(B)$, where $E_F(B)$ denotes the magnetic-field-dependent Fermi energy, energy shifts due to polaron effects occur.[29,30]

In Fig. 6(b) for the same geometry results on p-type $Pb_{1-x}Mn_xTe$ are shown, obtained from the analysis of magnetoreflectivity data taken with Fourier transform spectroscopy. Since the mobility of the p-type samples is lower, the transitions $n^+\rightarrow(n+1)^+$, $n^-\rightarrow(n+1)^-$ cannot be resolved. The calculated transition energies, based on the parameters from Tables I and II which were obtained from optimum fits to the interband and the g-factor data (see Sec. V) are in reasonable agreement with the observed ones.

In Voigt geometry $\mathbf{E}\|\mathbf{B}$, experiments were performed again on n- and p-type samples with $\mathbf{B}\|[1\bar{1}0]$, i.e., $\Phi=35.26°$ and $\Phi=90°$. For the PbTe band structure just the oblique valley cyclotron resonance ($\Phi=35.26°$) is allowed, whereas no cyclotron transition is possible for the two $\Phi=90°$ valleys. In Fig. 7 FIR transmission experi-

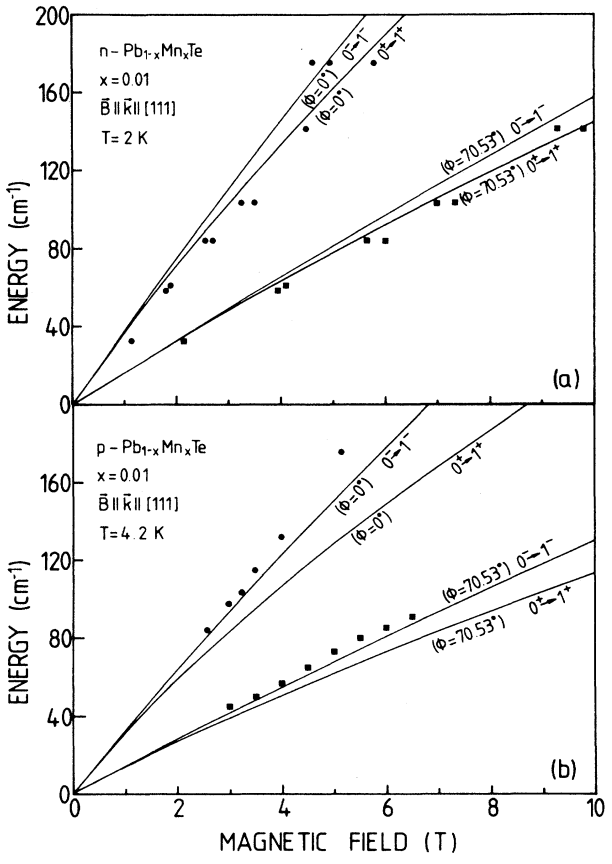

FIG. 6. (a) (Upper half): Intraband magneto-optical transition energies as derived from cyclotron resonances for infrared experiments in Faraday geometry. Two kinds of resonances associated with the $\Phi=0°$ (●) and $\Phi=70.53°$ (■) valleys are observed. Solid lines: calculated data. (b) (Lower half): as in (a) but for a p-type $Pb_{1-x}Mn_xTe$ ($x=0.01$) sample. Due to lower mobilities the two different transitions $1^-\rightarrow0^-$, $1^+\rightarrow0^+$ are not resolved experimentally.

ments on n-type PbTe and n-type $Pb_{1-x}Mn_xTe$ are compared with each other. A strong second resonance is observed at fields higher than the cyclotron-resonance transition. As already shown in Refs. 23 and 12, the second resonance exhibits a strong temperature dependence and vanishes at higher temperatures. Zawadzki[12,31] has calculated magneto-optical intraband selection rules based on the exchange contribution, treating the nondiagonal exchange terms as a perturbation. The nondiagonal terms mix the conduction spin states as well as the valence spin states and enhance additional combined spin-flip resonances as well as pure spin-flip resonances. In PbTe-like materials without magnetic ions such resonances are very weak since they result from far band interactions only. The observed transitions for several FIR laser lines are summarized in Fig. 8(a) together with calculated data (based on the parameters of Tables I and II). From these data the additional transition seems to be a spin-flip resonance in the oblique ($\Phi=35.26°$) valleys.

Similar FIR results in Voigt geometry $\mathbf{E}\|\mathbf{B}\|[1\bar{1}0]$ for p-type $Pb_{1-x}Mn_xTe$ ($x=0.01$) are qualitatively different as shown in Fig. 8(b). Again a cyclotron resonance of the holes of the oblique valley ($0^- \rightarrow 1^-, \Phi=35.26°$) is observed together with an additional resonance which is only observable for fields in excess of 2.5 T by Fourier transform spectroscopy and may be hidden for lower fields due to the dielectric anomaly associated with the cyclotron resonance $0^- \rightarrow 1^-$. In Fig. 8(b) several transitions are calculated as indicated. A spin-flip transition ($0^- \rightarrow 0^+$) of the oblique ($\Phi=35.26°$) valleys would be indistinguishable from their cyclotron resonance, a combined spin flip (CSF, $0^- \rightarrow 1^+$) for the $\Phi=90°$ valleys deviates at higher fields. Therefore the additional resonance in p-type $Pb_{1-x}Mn_xTe$ is likely to be a spin-flip resonance of the $\Phi=90°$ valleys.

Further experimental investigations, especially on the temperature dependence of the observed resonances in Voigt geometry in p-type $Pb_{1-x}Mn_xTe$ are necessary to obtain a more complete understanding. In addition calculations on the oscillator strength of the transitions involving spin flip are necessary for comparison as well.

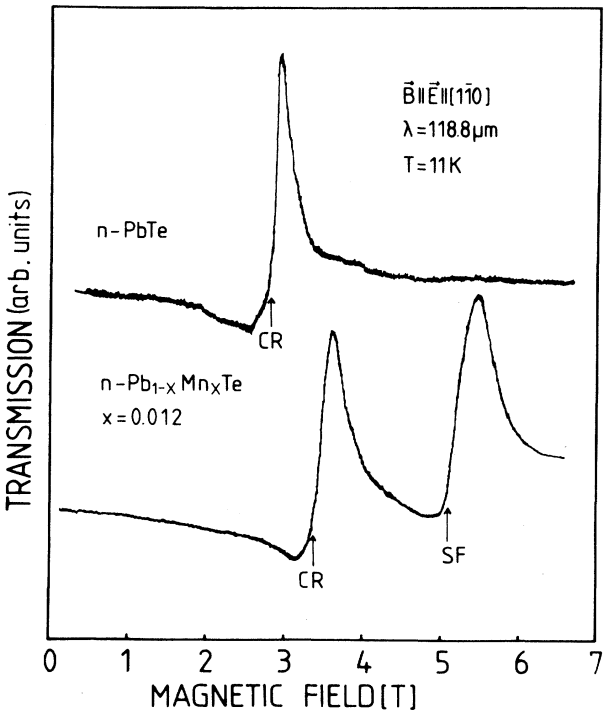

FIG. 7. Far-infrared transmission in Voigt geometry $\mathbf{E}\|B\|[1\bar{1}0]$. In PbTe just the oblique valley resonance ($\Phi=35.26°$) is observed, whereas in $Pb_{1-x}Mn_xTe$ an additional resonance identified as spin-flip resonance occurs.

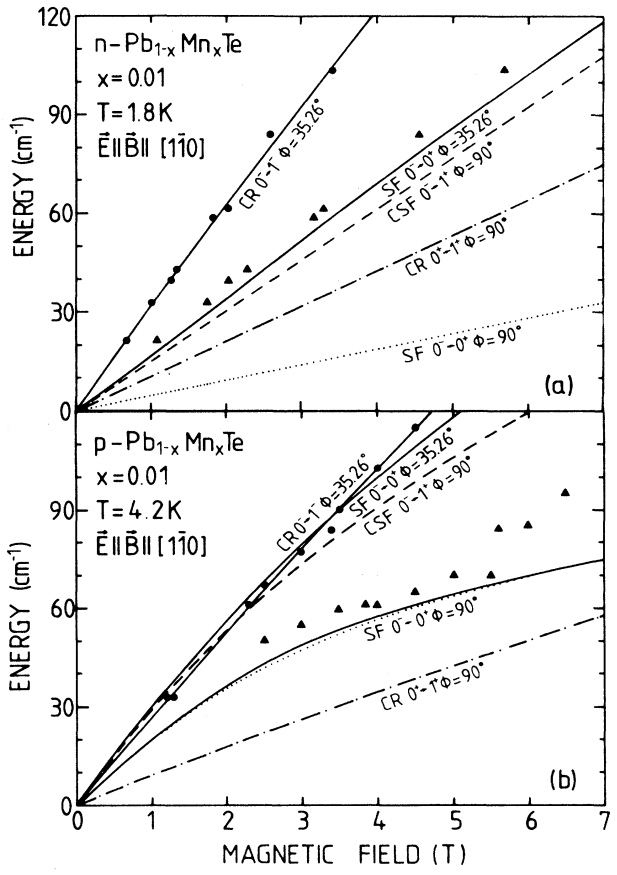

FIG. 8. (a) (Upper half): Experimental (●, ▲) and calculated resonance positions in Voigt geometry ($\mathbf{E}\|\mathbf{B}\|[1\bar{1}0]$) for n-type $Pb_{1-x}Mn_xTe$ together with identification. CR, Cyclotron resonance; SF, spin resonance; CSF, combined spin-flip resonance. (b) (Lower half): As in (a) but for p-type $Pb_{1-x}Mn_xTe$ ($x=0.01$) at $T=4.2$ K. Experimentally observed transitions correspond to cyclotron resonance (●) in the oblique valleys and to spin-flip resonance (▲). The bowing is due to strong effect of exchange interaction.

C. CARS experiments

Figure 9(a) shows experimental data on the CARS intensity for $\Delta\omega=\omega_L-\omega_s=34.3$ cm^{-1} as a function of magnetic field. The arrows indicate the resonance positions and (*a*) corresponds to the spin flip of photoexcited electrons in the $\Phi=90°$ valley. Both of the spin-flip transition of holes [(*b*), $\Phi=90°$, (*d*), $\Phi=35.26°$] are observable. The spin-flip resonance of photoexcited electrons for the $\Phi=35.26°$ valleys (*c*) is not observed at $T=1.8$ K since it coincides almost with that of the holes (*b*), which is much stronger in the *p*-type sample. However, as the temperature is changed (*c*) is observable and in Fig. 9(b) the resonance positions are shown for the identical $\Delta\omega=34.3$ cm^{-1} as a function of T. Apparently, the spin-flip resonances of the electrons (*c*),(*a*) shift only slightly with increasing temperature to somewhat *smaller* magnetic fields whereas the situation is opposite for the valence band. The spin-flip resonance for the holes (*d*) and (*b*) shift drastically to higher magnetic fields as the temperature is increased. This shift is particularly pronounced for the $\Phi=90°$ valley [resonance (*b*)].

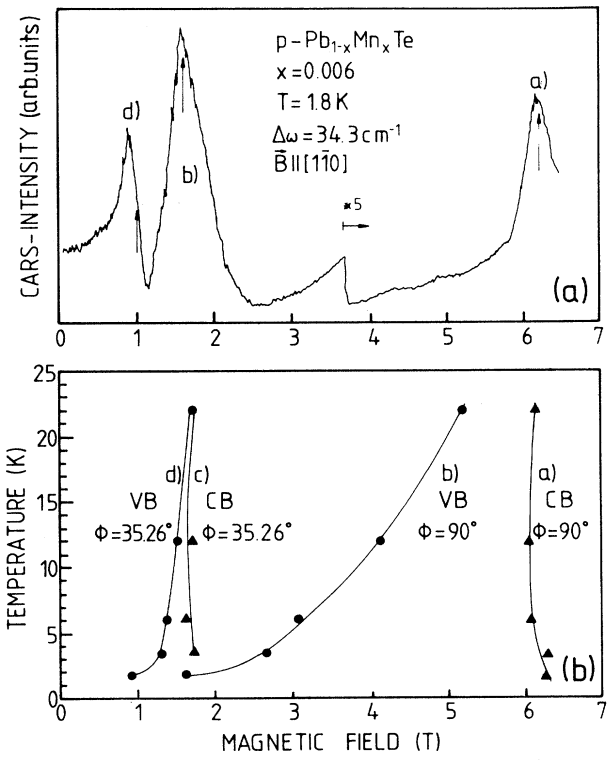

FIG. 9. (a) (Upper half): CARS intensity vs magnetic field for $\Delta\omega=34.3$ cm^{-1} at $T=1.8$ K. The transitions marked (a), (b), (d) correspond to spin flip of electrons ($\Phi=90°$) and of holes ($\Phi=90°$, $\Phi=35.26°$), respectively. Arrows indicate resonance positions. (b) (Lower half): Temperature dependence of CARS intensity resonances for both electrons and holes in the $\Phi=35.26°$ and $\Phi=90°$ valleys.

Recordings as plotted in Fig. 9(a) were taken for a large number of laser frequencies with different $\omega_L-\omega_S=\Delta\omega$. In Figs. 10(a)–10(c) results on three samples with $x=0.006$, $x=0.008$, and $x=0.01$ at $T=1.8$ K are summarized. From an inspection of the data it fol-

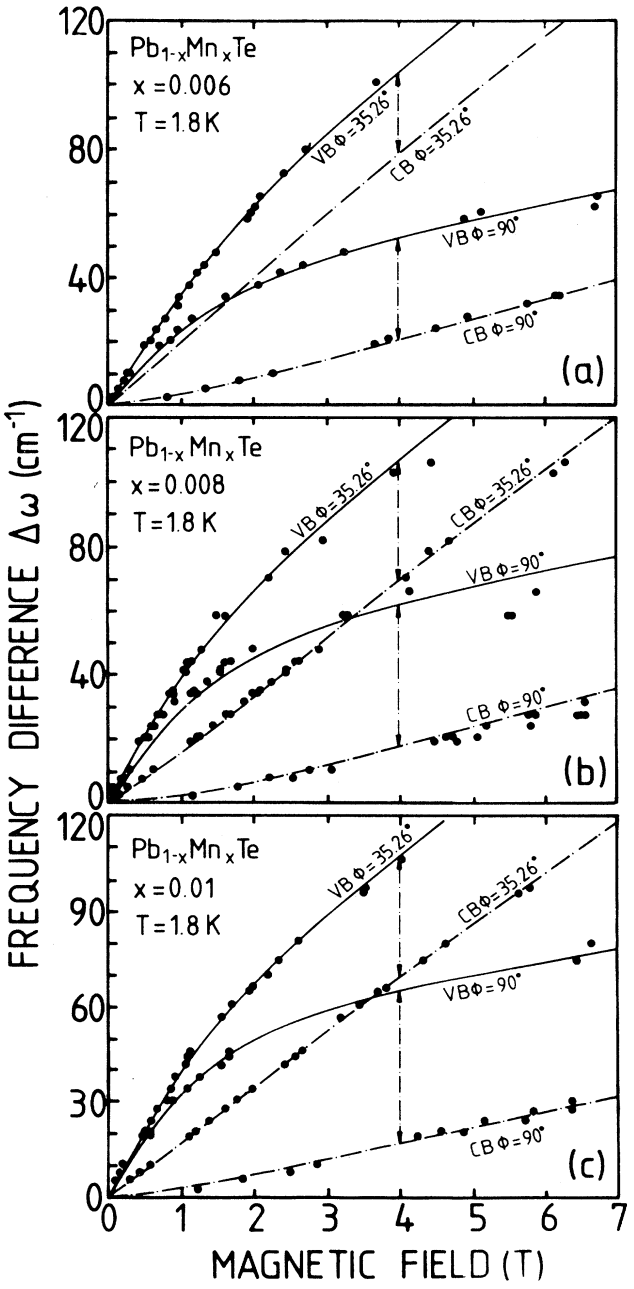

FIG. 10. Results of CARS measurements (frequency differences) as a function of magnetic field for $x=0.006$ (a), $x=0.008$ (b), and $x=0.01$ (c) for $\mathbf{B}\|[1\bar{1}0]$ and $T=1.8$ K. Experimental data: ●, calculated data for holes; solid lines for $\Phi=35.26°$ and $\Phi=90°$ valleys; for electrons, dashed-dotted lines for $\Phi=35.26°$ and $\Phi=90°$ valleys.

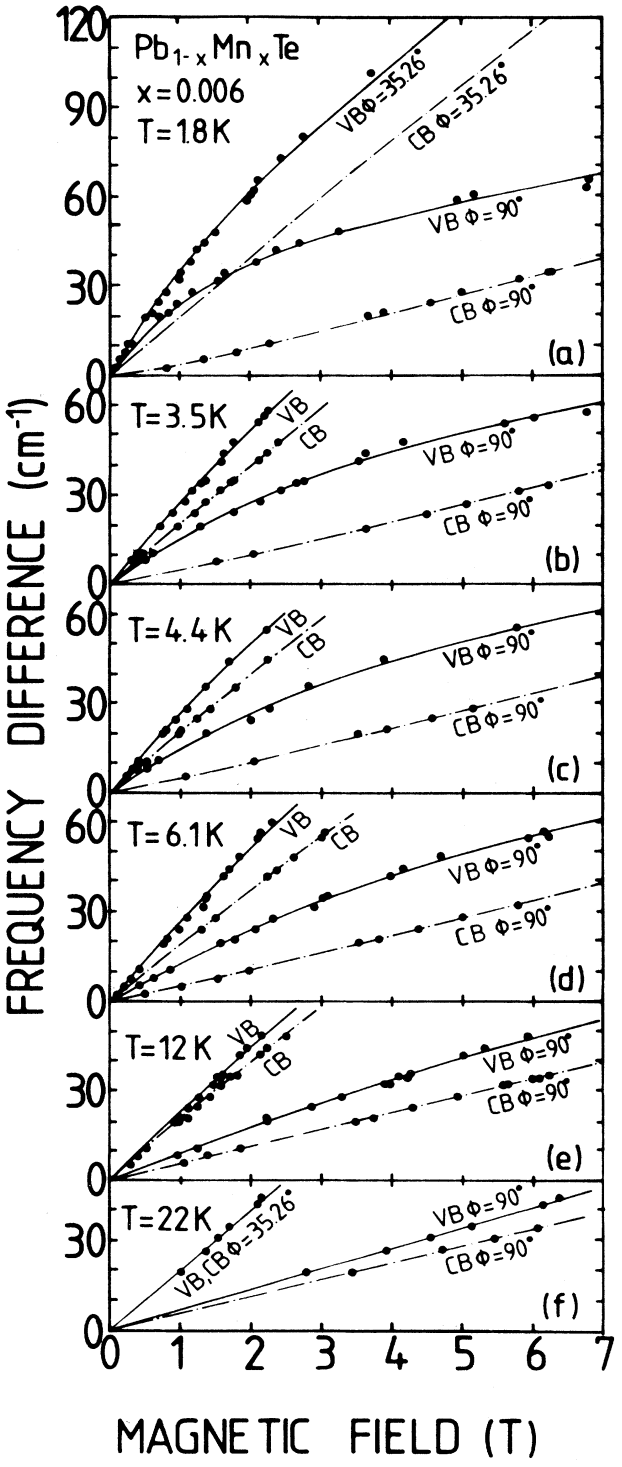

FIG. 11. Results of CARS measurements on $Pb_{1-x}Mn_xTe$ ($x=0.006$) for six different temperatures (a)–(f). Experimental data ●; calculated data, solid lines for holes ($\Phi=90°$, $\Phi=35.26°$) and dashed-dotted lines for electrons ($\Phi=90°$, $\Phi=35.26°$).

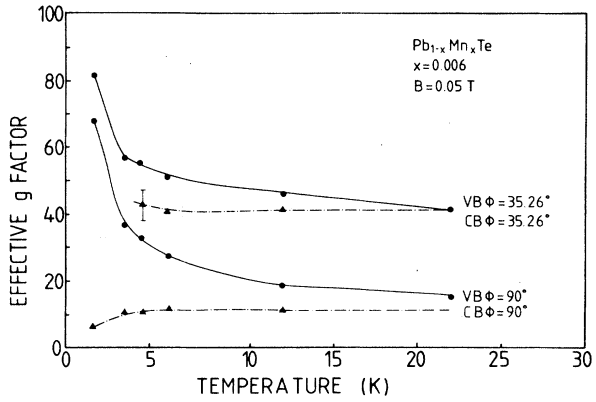

FIG. 12. Temperature dependence of effective electron (▲) and hole g factors (●) for a magnetic field of $B=0.05$ T as derived from CARS experiments. The solid and dashed-dotted lines are just a guide to the eye.

lows that (i) the contributions to the spin-flip transition energies induced by the exchange interaction are much larger for the valence band than for the conduction band; (ii) for fields in excess of about 2 T, the difference between the spin-flip energies for electrons and holes for the oblique $\Phi=35.26°$ valleys as well as for the $\Phi=90°$ valleys changes only slightly with field [arrows in Figs. 10(a)–10(c)]. This energy difference is the same within experimental error which is observed for interband magneto-optical transitions in $\mathbf{B}\|\mathbf{k}$ geometry if energy differences for the σ^+ and σ^- polarized radiation [0^-(VB)$\rightarrow 0^+$(CB), 0^+(VB)$\rightarrow 0^-$(CB)] are derived from the experimental data.

The calculated transition energies are presented by the solid lines in Figs. 10(a)–10(c) using the model outlined in Sec. II. Actually, the four exchange parameters listed in Table II as well as T_0 were determined from the fits shown in Figs. 10(a)–10(c), whereas the two band parameters $P_\perp$, $P_\parallel$ and the energy gap were obtained from the magneto-optical interband transition energies. The far band parameters were assumed to be identical to those of PbTe.

The temperature dependence of these transition energies is quite dramatic, as shown in Figs. 11(a)–11(f) for experiments performed up to 22 K for a sample with a Mn content of $x=0.006$. This fact is particularly pronounced for the hole–spin-flip transitions. With increasing lattice temperature the sequence of spin-flip transition energies becomes more and more PbTe-like apart from the fact that the absolute values of the g factors are smaller due to the larger gap. In Fig. 12 the effective electron and hole g factors (calculated from the experimental spin-flip energies at $B=0.05$ T are shown as a function of temperature in the range 1.8–22 K). For $\mathbf{B}\|[1\bar{1}0]$ two conduction- and two valence-band g factors are shown. The most dramatic temperature shifts exhibits the g factor for the $\Phi=90°$ VB valleys. The photoexcited electrons in the $\Phi=35.26°$ valleys are barely visible for this Mn content.

V. DISCUSSION

A. Band and exchange parameters

In order to obtain the band and exchange parameters and their dependence on Mn content, which are listed in Tables I and II, the following procedure was performed. To determine the two band parameters like the minimum energy gap, the two band momentum matrix elements $2P_{\perp}^2/m_0$ and $2P_{\parallel}^2/m_0$, fits to the magneto-optical interband transitions were made with the far band parameters m_t^+, m_l^+, g_l^+, g_t^+ assumed to be identical to those of PbTe (which were taken from Ref. 24). This assumption seems to be valid for the rather small Mn content ($x<0.02$) of the samples under investigation. It means that neither the band ordering nor the energy separation for the two higher conduction and two lower valence levels at the L point of the Brillouin zone changes considerably when Mn is introduced into the PbTe lattice, for such small x values.

From the fits to the interband data it follows that with increasing Mn content $2P_{\perp}^2/m_0$ decreases, whereas the anisotropy value $P_{\perp}^2/P_{\parallel}^2$ increases (see Table I). The exchange-induced coefficients A,a_1,B,b_1 as defined in Ref. 20 and T_0 are obtained from least-square fits to the experimentally observed $0^-\rightarrow 0^+$ transitions, i.e., from the CARS experiments which determine these spin splittings most accurately. Since in these experiments for $\mathbf{B}\|[1\bar{1}0]$ two kinds of valleys (i.e., $\Phi=35.26°$ and $\Phi=90°$) yield two g factors both for the conduction as well as for the valence band, all band and exchange parameters can be determined unambiguously. S_0 is taken from fits to the experimental magnetization data. In principle, from the four parameters A, a_1, B, and b_1 the four exchange integrals α,δ (VB) and $\beta_{\parallel},\beta_{\perp}$ (CB) (see Refs. 13 and 20) can be calculated if the spin-orbit-mixing parameters $\Theta^{\pm}$ (Refs. 32 and 33) were known with sufficient accuracy.

The exchange-induced effects in the valence band are larger than in the conduction band. The parameter $|A|$ decreases with increasing temperature which is astonishing. Such a drastic variation of an exchange parameter is a hint for a breakdown of the mean-field approach since it demonstrates that the temperature dependence of the hole g factors does not reflect the temperature dependence of the macroscopic magnetization.

It should be stressed that the numerical values of the spin splittings as derived from magneto-optical interband experiments in Faraday geometry in sufficiently high magnetic fields, which were already given partly in Ref. 13 for several samples with $0.006<x<0.017$ are in agreement with the spin splitting obtained here from the CARS experiments. The uncertainty of the determination of the spin splittings $E(n^+)-E(n^-)$ is much larger if interband transition data are used in comparison to the much more accurate spin-resonant four-wave-mixing data.

The far-infrared data on cyclotron and spin resonance were not used as input parameters to the fits. With the theoretical expressions as used, finite k_B values cannot be treated. Therefore the occupation effects, which are always present for the carrier concentrations in our samples (see also Ref. 29), cannot be considered properly. Thus the calculated transition energies based on parameters from the interband and CARS experiments were just compared with experimental far-infrared intraband magneto-optical data. The overall agreement is reasonable.

In the magneto-optical experiments in Voigt geometry (with $\mathbf{E}\|\mathbf{B}\perp\mathbf{k}$, $\mathbf{B}\|[1\bar{1}0]$, $\mathbf{k}\|[111]$) new transitions were found: In the interband data shown in Fig. 4(b), a new spin-flip transition $0^+(\mathrm{VB})\rightarrow 0^-(\mathrm{CB})$ was found induced by the Mn ions. In the intraband data again spin-flip transitions were found both in the conduction band as well as in the valence band (Fig. 8) besides the tilted-orbit cyclotron resonance in the $\mathbf{E}\|\mathbf{B}$ Voigt geometry. These observations demonstrate a modification of the selection rules brought about by the interaction between the localized Mn^{++} spins and the free electrons as well as holes. A calculation of the altered selection rules and their oscillator strengths is in progress.[31]

B. Effective electron and hole g factors

1. Magnetic-field dependence

The spin-resonant four-wave-mixing experiments provide an ideal means for the study of the magnetic-field dependence of the spin splitting between the 0^--0^+ states both in the conduction and in the valence bands. In order to check the mean-field approach used for the treatment of the exchange interaction in this many-valley semiconductor, in Fig. 13 experimentally derived g factors are plotted as a function of magnetic field together with calculated data.

For an $x=1\%$ sample, four g factors are experimentally accessible, two for the conduction and two for the

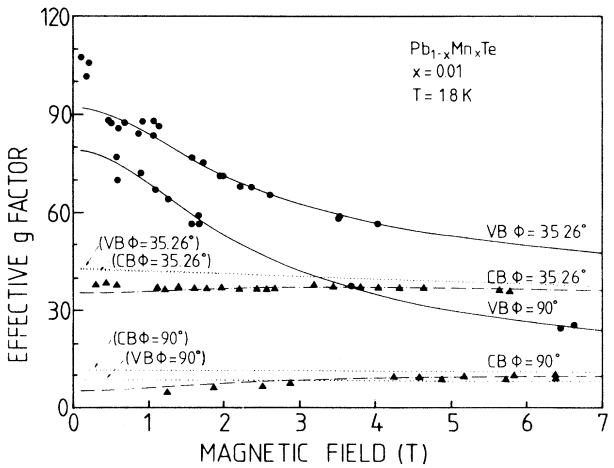

FIG. 13. Magnetic-field dependence of effective g factors derived from CARS experiments in $\mathbf{B}\|[1\bar{1}0]$ geometry (● holes, ▲ electrons) with theoretical data (solid lines for holes, dash-dotted lines for electrons including exchange interaction; dotted lines, without exchange interaction, i.e., B dependence resulting from nonparabolicity) for $Pb_{1-x}Mn_xTe$, $x=0.01$ at $T=1.8$ K.

valence band. The common features are the following. With increasing magnetic field the absolute values of the g factors (i) decrease in the valence band for both kinds of valleys; the relative change is larger for the $\Phi=90°$ valleys than for the $\Phi=35.26°$ valleys; and (ii) *increase* in the conduction band for both kinds of valleys, the relative increase being again stronger for the $\Phi=90°$ valleys.

The mean-field approach yields an excellent overall agreement for all four kinds of g factors involved. Only for very small fields the experimentally derived hole g factors are appreciably higher than the calculated ones.

In order to demonstrate the effect of the exchange interaction on the magnetic-field dependence of the effective g factors, we note that nonparabolicity decreases the g factors with increasing field for electrons and holes for all types of valleys. In Fig. 13 theoretical values of the magnetic-field dependence of the effective g factors are plotted with and without exchange interaction for $0^- \rightarrow 0^+$ transitions. With increasing field the effective electron g factors in the dilute magnetic material approach the values of the host material from *below*, whereas the actual hole g factors approach the corresponding g factors without taking into account the exchange interaction from *above*. Figure 13 shows that the exchange-induced effects in $Pb_{1-x}Mn_xTe$ are appreciably larger in the valence band as compared to the conduction band.

The actual exchange constants α, δ (CB) and $\beta_{\|},\beta_{\perp}$ (VB) were derived as a function of composition and temperature. In order to calculate these values the spin-orbit-mixing parameters $\Theta^{\pm}$ (Ref. 32) as given by Bernick and Kleinman are used.[33] The large absolute value of δ is most probably an artifact caused by the uncertainty of $\sin\Theta^+$ (Ref. 33) and a small change of this parameter drastically affects the value of δ. Unfortunately, even the general uncertainty in the spin-orbit-mixing parameters $\Theta^{\pm}$ is too large to derive reliable values for α, δ (VB) and $\beta_{\|},\beta_{\perp}$ (CB).

2. *Temperature dependence*

In Fig. 12 the temperature dependence of the effective electron and hole g factors is presented. At a first glance, it seems that also the temperature dependence of the spin splitting is accounted for by the mean-field theory, i.e., by the temperature dependence of the macroscopic magnetization. However, from fits similar to those presented in Figs. 10(a)–10(c) to CARS data taken at various temperatures apparently the exchange parameters are not constant. The parameter A shows the most drastic variation changing from -225 meV at $T=1.8$ K to -50 meV at $T=12$ K. Even in the small temperature interval from 1.9 K to 4.4 K the decrease of $|A|$ is about a factor of 2.

If the MFA would entirely determine the temperature dependence, then the observed energy difference ΔE between the spin splitting of the valence states minus the spin splitting of the conduction states normalized to the magnetization M would be constant, i.e., independent of T. In Fig. 14 this ratio $\Delta E/M$ decreases significantly with increasing T. This effect is mainly caused by a temperature dependence of the parameter A as given in Table II and shown in the insert of Fig. 14.

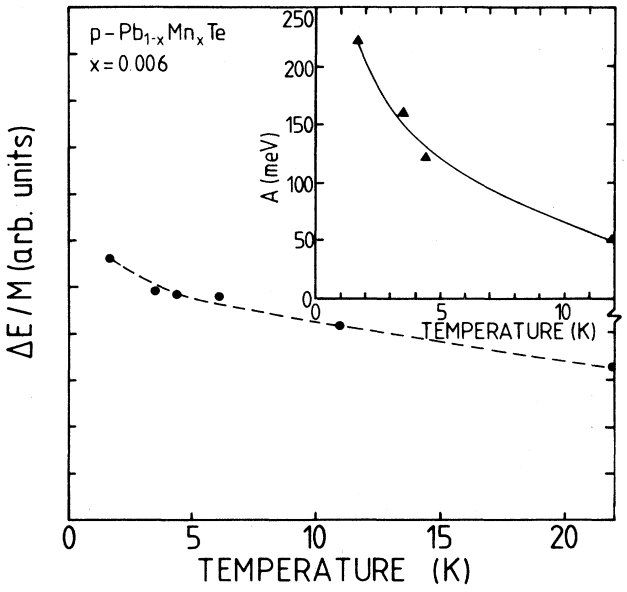

FIG. 14. Energy difference ΔE = spin splitting in the valence minus spin splitting in the conduction band, divided by magnetization as a function of temperature for $Pb_{1-x}Mn_xTe$, $x=0.006$. Insert: Temperature dependence of the exchange parameter A.

Of course, the variation of the exchange parameters with temperature remains to be explained and suggests that further modifications of the theory are necessary.

VI. CONCLUSIONS

In the past several magneto-optical experiments performed in the field range above 1 T were interpreted as giving evidence for a vanishing spin splitting of the valence band at $B \rightarrow 0$ T in $Pb_{1-x}Mn_xTe$.[13,16] This conclusion was mainly based on interband data which were extrapolated to zero magnetic field.

However, the CARS experiments performed in the magnetic-field range down to 0.05 T conclusively show that the spin-flip transition energies tend actually to zero, not only for the conduction band, but also for the valence band for vanishing magnetic fields. With the aid of the mean-field approach and with the use of experimental magnetization data, the observed magneto-optical transitions can be well understood. In this respect the only difference to $Hg_{1-x}Mn_xTe$ with similar Mn contents is the simple fact that the exchange interaction in the narrow-band-gap IV-VI compound is considerably weaker than that in $Hg_{1-x}Mn_xTe$.

The experiments presented here and their interpretation yield further details on dilute magnetic (semimagnetic) semiconductors in a class of materials where the host lattice is not of zinc-blende but of the rock-salt structure with bond angles of 90°. Recently Gorska and Anderson[17] have determined the nearest-neighbor (NN) exchange constants in several IV-VI compounds containing manganese, including $Pb_{1-x}Mn_xTe$. From high-

temperature susceptibility measurements it turned out that these NN exchange constants are of the order of 1 K only which is about a factor of 10 smaller than those found in dilute magnetic II-VI compounds. Estimations based on the Anderson superexchange mechanism have shown that indeed the difference in the crystalline structure between II-VI and IV-VI compounds leads to an order-of-magnitude difference in the exchange interaction with superexchange via the anions as the dominant mechanism.[17]

In view of the rather small exchange constants for the mobile-carrier—Mn-ion interaction and the fact that these constants depend considerably on temperature, it is not astonishing that only for very low temperatures and low magnetic fields strong "semimagnetic" effects are found, i.e., a strong dependence of the energy of spin-split states on temperature and magnetic field. These effects are much stronger for holes than for electrons and of opposite sign. The temperature dependence of the exchange parameters warrants further investigation.

Note added in proof. Zasavitskii *et al.*[35,36] have recently studied the spin splitting in semimagnetic IV-VI semiconductors by photoluminescence techniques.

ACKNOWLEDGMENTS

We thank Professor W. Zawadzki, Dr. E. Bangert, and Professor H. G. Häfele for discussions, S. Gerken and I. Roschger for early experimental contributions, G. Elsinger, J. Vlcek, and L. Palmetshofer for the samples. Part of the far-infrared spectroscopic experiments were performed at the Hochfeld Magnetlabor, Max-Planck-Institut, Grenoble. This work was supported by the Deutsche Forschungsgemeinschaft (Bonn, Germany) and the Fonds zur Förderung der wissenschaftlichen Forschung (No. P6928) (Vienna, Austria).

[1]J. K. Furdyna, J. Appl. Phys. **64**, R29 (1988), and references cited therein.

[2]G. Bauer, Mat. Res. Soc. Proc. **89**, 107 (1987) (edited by R. L. Agrawal, J. K. Furdyna and S. von Molnar).

[3]D. L. Partin, IEEE J. Quantum Electron. **QE-24**, 1716 (1988).

[4]P. Norton and M. Tacke, J. Cryst. Growth **81**, 405 (1987).

[5]J. R. Anderson and M. Gorska, Solid State Commun. **52**, 601 (1984).

[6]G. Karczewski, M. von Ortenberg, Z. Wilamowski, W. Dobrowolski, and J. Niedwodniczanska-Zawadzka, Solid State Commun. **55**, 249 (1985).

[7]G. Braunstein, G. Dresselhaus, J. Heremans, and D. L. Partin, Phys. Rev. B **35**, 1969 (1987).

[8]T. Story, R. R. Galazka, R. B. Frenkel, and P. A. Wolff, Phys. Rev. Lett. **56**, 777 (1986).

[9]H. J. M. Swagten, W. J. M. de Jonge, R. R. Galazka, P. Warmenbol, and J. T. Devreese, Phys. Rev. B **37**, 9907 (1988).

[10]H. Pascher, P. Röthlein, and M. Tacke, in *Proceedings of the 19th International Conference on the Physics of Semiconductors, Warszawa, 1988,* edited by W. Zawadzki (Polish Academy of Sciences, Warszawa, Poland, 1988), p. 1591.

[11]J. Niedwodniczanska-Zawadzka, J. Kossut, A. Sandauer, and W. Dobrowolski, in *Physics of Narrow Gap Semiconductors,* Vol. 152 of *Lecture Notes in Physics,* edited by E. Gornik, H. Heinrich, and L. Palmetshofer (Springer, Berlin, 1982), p. 326.

[12]J. Niedwodniczanska-Zawadzka, J. G. Elsinger, L. Palmetshofer, A. Lopez-Otero, E. J. Fantner, G. Bauer, and W. Zawadzki, Physica B+C, **117&118B**, 458 (1983).

[13]H. Pascher, E. J. Fantner, G. Bauer, W. Zawadzki, and M. v. Ortenberg, Solid State Commun. **48**, 461 (1983).

[14]G. Karczewski and L. Kowalczyk, Solid State Commun. **48**, 653 (1983).

[15]G. Karczewski and M. von Ortenberg, in *Proceedings of the 17th International Conference on the Physics of Semiconductors, San Francisco, 1984,* edited by J. D. Chadi and W. A. Harrison (Springer, New York, 1985), p. 1435.

[16]M. von Ortenberg, Solid State Commun. **52**, 111 (1984).

[17]M. Gorska and J. R. Anderson, Phys. Rev. B **38**, 9120 (1988).

[18]M. S. Adler, C. R. Hewes, and S. D. Senturia, Phys. Rev. B **7**, 186 (1973).

[19]R. R. Galazka and J. Kossut, in *Narrow Gap Semiconductors: Physics and Applications,* Vol. 133 of *Lecture Notes in Physics,* edited by W. Zawadzki (Springer, Berlin, 1980), p. 245.

[20]H. Pascher, P. Röthlein, G. Bauer, and L. Palmetshofer, Phys. Rev. B **36**, 9395 (1987).

[21]H. Pascher, P. Röthlein, I. Roschger, G. Bauer, in Ref. 10, p. 1535.

[22]G. Elsinger, L. Palmetshofer, and A. Lopez-Otero, Nuovo Cimento **2D**, 1869 (1983).

[23]G. Bauer, in *Physics of Semiconducting Compounds,* edited by R. R. Galazka (Ossolineum, Warszawa, 1983), p. 62.

[24]H. Pascher, Appl. Phys. **B34**, 107 (1984).

[25]C. K. N. Patel, R. E. Slusher, and P. A. Fleury, Phys. Rev. Lett. **17**, 1011 (1966).

[26]M. Gorska, T. Wojtowicz, and W. Knap, Solid State Commun. **51**, 115 (1984).

[27]M. von Ortenberg, G. Bauer, and G. Elsinger, Proceedings of the International Conference on Millimeter Waves, Marseille, 1985 (unpublished).

[28]G. Bauer, in Ref. 19, p. 427.

[29]H. Burkhard, G. Bauer, and W. Zawadzki, Phys. Rev. B **19**, 5149 (1979).

[30]P. Vogl and P. Kocevar, in *Proceedings of the International Conference on the Physics of Semiconductors, Edinburgh, 1978,* Institute of Physics Conference Series No. 43, edited by R. H. Wilson (I.O.P., London, 1978), p. 1317.

[31]W. Zawadzki (unpublished).

[32]D. L. Mitchell and R. F. Wallis, Phys. Rev. **151**, 581 (1966).

[33]R. L. Bernick and L. Kleinman, Solid State Commun. **8**, 569 (1970).

[34]A. Golnik and J. Spalek, J. Magn. Magn. Mater. **54-57**, 1207 (1986).

[35]I. I. Zasavitskii, L. Kowalczyk, B. N. Matsonashvili, and A. V. Sazonov, Fiz. Tekh. Poluprovodn. **22**, 2118 (1988) [Sov. Phys.—Semicond. **22**, 1338 (1988)].

[36]I. I. Zasavitskii and A. V. Sazonov, Fiz. Tverd. Tela **30**, 1669 (1988) [Sov. Phys.—Solid State **30**, 962 (1988)].